POLYMER AND STAINLESS STEEL-BASED 3D MICROELECTRODE ARRAYS (3D MEAS), WITH PENTA-MODAL SENSING CAPABILITIES FOR THE INVESTIGATION OF ELECTROGNIC CELLS

Charles M. Didier[1,†], *Julia Freitas Orrico*[1,†], *Omar S. Cepeda-Torres*[1,2,†], *Aliyah Baksh*[1], *Jorge Manrique Castro*[1] *and Swaminathan Rajaraman*[1]

[1] University of Central Florida, Orlando, FL, USA, [2] Polytechnic University of Puerto Rico, San Juan, PR

[†] Equally Contributing Authors

ABSTRACT

Benchtop tissue cultures have historically provided major breakthroughs in biological research. Modern "on-a-chip" and Microphysiological Systems (MPS) demand integrated sensing/stimulation modalities, to produce complex, multiplexed datasets. To this end, novel fabrication strategies incorporating readily available materials, including polymers and steel alloys, are exciting avenues for the development of such multifunctional biosensors. Here, we showcase a Penta-Modal biosensor platform, which incorporates a transparent polymer substrate (for cellular image analysis), stainless steel (SS) 3D microelectrode array (3D MEA) structures, with an included 3D microfluidic adaptation, and both temperature and analyte sensing capabilities all on a single chip. Together, this device demonstrates the potential for a highly versatile data collection regimen, in a compact one-chip platform.

KEYWORDS

Multi-Modal Biosensor, Optical Clarity, 3D Microelectrode Array (3D MEA), Interdigitated Electrodes, Analyte Sensor, Temperature Sensor, Transmitted Light Microscopy

INTRODUCTION

In vitro organ-on-a-chip models have become one of the most exciting emerging technologies. Built at the intersection of micro/nanoengineering and cellular biology, specialized arrangements of living cells are better able to simulate physiology at the cellular, tissue and organ level **[1,2].** Recent complexities of these models demand a balance of sensing and stimulation modalities, and strategies for procuring multifaceted, long-term datasets **[1]**. This is especially relevant with respect to MPS, which integrate complex biology, various materials with advanced sensors, and require unprecedented combinatorial biological detail to evaluate *in vitro* systems (ex. brain, heart, or muscle) seamlessly in the same platform, producing more physiologically relevant datasets. 3D MEA sensors have become highly desired as advanced sensors in MPSs for obtaining electrophysiological signals from electrically active cells, networks, and complex assemblies **[3,4]**. For many MPS, 3D MEAs can form the base of the sensing/stimulation platforms on to which other sensing modalities can be integrated **[4]**.

These other modalities include potentially 2D/3D microfluidics, which may be utilized to chemically stimulate cells whose response is further monitored through transparent/optical means (transparency to enable high content assays can be thought of as another sensing modality). Additionally, temperature control and maintaining homeostasis are vital in efforts to address MPS interfacing outside of an incubator environment **[5]**. For precise control of cellular growth and health, key analyte detection would also allow for maintenance of cellular homeostasis **[6]** and could additionally be utilized in combination with 2D/3D microfluidics to detect culture health during chemical stimulation. Thus electrochemical, electrophysiological, and temperature sensing/stimulation, along with transparency and microfluidic-mediated assays allow for a ***total of five sensing/stimulation modalities*** which are achieved on a single chip **[2-9]**. Our prior work demonstrated a tri-modal, polymer 3D MEAs (*electrical, optical, and microfluidics*) **[3]**.

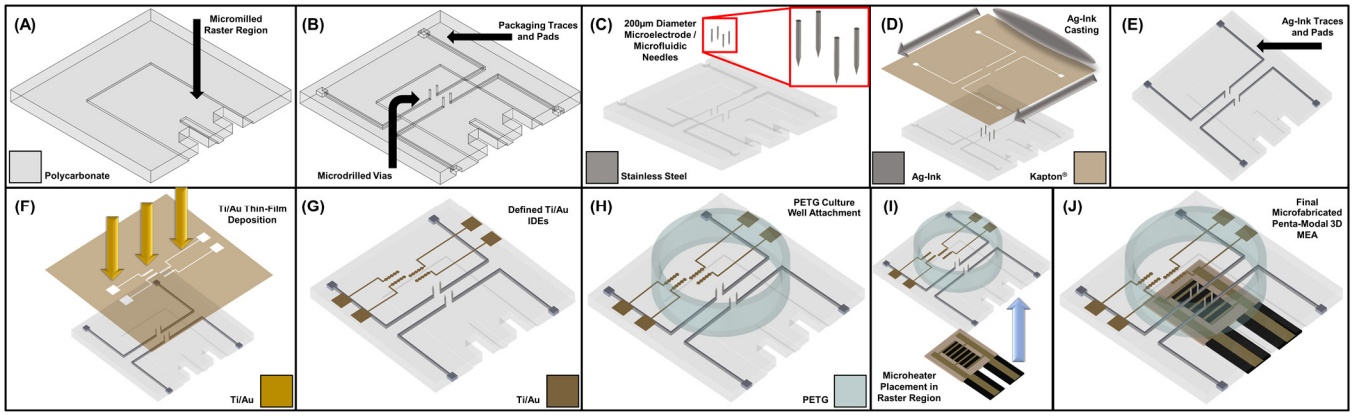

Figure 1: *Process flow schematic for the fabrication of the Penta-Modal biosensor. (A) Micromilled bulk polycarbonate (PC) with a raster-region with a thin cut-out where the microheater is to be placed. (B) Micromilling and microdrilling of packaging traces, pads, and through-vias respectively. (C) Magnetic-assisted insertion of microneedles to define the bulk 3D MEA structure. (D) Precision Silver (Ag)-ink casting of the traces, pads and vias from (C), utilizing a laser micromachined Kapton® mask. (E) Final cured Ag-ink, defining the functional packaging for the 3D MEA sensing modality. (F) Thin-film, electron beam deposition of Titanium (Ti) / Gold (Au) IDEs and contact pads, for the temperature and analyte-sensing modalities. (G) Final defined IDEs on the top surface of the polycarbonate substrate. (H) PET-G culture well attachment with 10:1 polydimethylsiloxane (PDMS). (I) Microheater placement into the raster-region on the underside of the substrate. (J) Final fabricated Penta-Modal 3D MEA biosensor platform.*

978-1-940470-04-7/HH2022/$25©2022TRF
DOI 10.31438/trf.hh2022.34

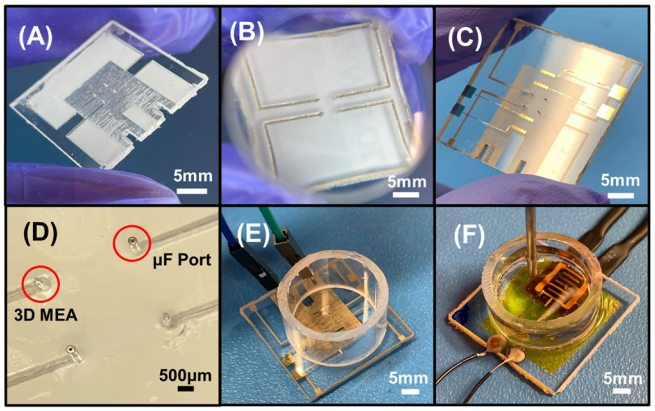

Figure 2: *Optical images detailing selected fabrication stages of the Penta-Modal biosensor from Figure 1. (A) Optical image corresponding to Figure 1B. In this image, the protective film is left partially in place to better contrast each micromilled, microdrilled, or microrastered element. (B) Optical image corresponding to Figure 1E. The cured Ag-ink is precision aligned to reside within the desired packaging traces and pads. (C) Optical image corresponding to Figure 1G. Both Ti/Au IDEs for the thermal and analyte sensor have been deposited, and ink-cast tracing leading to the inserted 3D MEAs can be observed, along with the microrastered microheater region. (D) Close-up optical image of the central device region from (C). Microfluidic (μF) ports are a facile substitution or addition to the 3D microelectrode insertion vias, and additional microfluidic ports may be added elsewhere in the culturing area. (E) Optical image of the culture well attachment fabrication step from Figure 1H. (F) Optical image of a fabricated biosensor from Figure 1J. In this image, the microheater is attached in the micro-raster-region for testing the devices' temperature sensing capabilities.*

Herein we expand this platform, by demonstrating a biosensor which additionally encompasses temperature and analyte-sensing, to provide a ***Penta-Modal Sensing Platform for Electrogenic Cellular Constructs***, towards procuring comprehensive MPS data analytics.

MATERIALS AND METHODS

A 24mm (length) by 24mm (width) by 1.75mm (thick) substrate was micromilled from bulk polycarbonate (T-Tech, USA; **Figure 1**). Within this substrate, a 300μm (length) by 300μm (width) by 300μm (depth) volume was microrastered on the back of the chip for microheater placement (**Figure 1A**). Subsequently, packaging areas were defined utilizing 1mm^2 contact pads and 200μm (width) traces (**Figure 1B**). Additionally, 220μm (diameter) by 500μm (depth) vias were microdrilled. All the micromilling/microdrilling was performed in a single step. Stainless steel (SS) needles (DBC^{TM}, South Korea; 200μm diameter) were trimmed to 1.85mm (height) and inserted utilizing magnetic insertion **[3]** to define 3D microelectrodes/microfluidic ports with a functional height of ~100μm (**Figure 1C**). Traces were defined with conductive Ag-ink (MasterBond, USA) casting before curing at 60°C for 24-hours (**Figure 1D**). A 750μm pitch circle-in-line geometry Kapton® (DuPoint, USA; 25μm thick) shadow mask was UV-laser micromachined (QuikLaze, USA) and Titanium (Ti; 100nm) / Gold (Au; 400nm) Interdigitated Electrodes (IDE) were defined through these masks with electron-beam deposition (Thermionics, USA). Next, a 16mm (inner diameter) by 5mm (height) PET-G culture well was attached with PDMS (Dow Corning, USA). A resistive micro-heater (Pelonis Technologies, USA: 1.05μA compliance/0.5-7V voltage) was subsequently affixed to the microrastered volume on the backside of the chip. IR imaging (Perfect Prime, USA) validated expected temperatures (results not shown). Full spectrum (100Hz-40MHz) impedance/phase were obtained utilizing Bode 100 (Omicron Labs, USA), for all impedance-based measurements. Root Mean Square (RMS) noise measurements were obtained using the Axion BioSystems MUSE® electrophysiological system (Axion Biosystems Inc., USA). Approximately, 1:100 dilutions of anti-L-Glutamine antibodies (Abcam, UK) were created in Dulbeccos phosphate buffered saline (Sigma, USA; DPBS). Mixed air plasma treatment (Plasma Etch, USA; 20s) was applied on analyte IDEs, prior to the deposition of 40μl of the diluted antibody, which was subsequently incubated at 22°C for 1-hour, and then removed before gentle cleaning with DPBS. A volume of 0.2-20mM L-Glutamine was utilized to assess the conjugated sensor's capabilities. Imaging of various aspects of the device was performed with Atomic Force Microscopy (AFM, Veeco, USA; tapping mode), Scanning Electron Microscopy (SEM, Zeiss, Germany), and optical imaging (iPhone XS; Apple, USA). Cell culture assays were performed utilizing C2C12 myocyte cells (ATCC, USA), with imaging occurring at 5 days *in vitro* (DIV). Cellular imaging was performed on the Keyence BZ-X810 confocal microscope (Keyence, Japan), and fluorescent live/dead confirmation staining was performed utilizing a standard Calcein AM / Propidium Iodide kit (Thermo Fisher Inc., USA).

RESULTS AND DISCUSSIONS

To achieve the "Penta-Modality" of the device, previously studied optical clarity, 3D microfluidics, and 3D microelectrode performance **[3]**, along with temperature and analyte sensing are demonstrated (**Figure 2**). 3D MEA impedance and phase sweeps (**Figure 3 A&B** respectively) were obtained across the full 10Hz-40MHz frequency spectrum utilizing electrochemical impedance spectroscopy (EIS). The biologically relevant 1kHz value, indicated an impedance of **2.76 kΩ**, and a phase signature of **-55°,** which are well within literature defined values **[9,10]**. This phase signature implies a more capacitive dominance of the circuit at the critical electrophysiologically relevant frequency of 1 kHz, however examination of the Nyquist plot for this data is necessary to precisely determine other properties of the 3D microelectrode. The averaged RMS noise before and after addition of DPBS are indicated as an inset in **Figure 3A**. The values were reduced from an average of **18.26 μV** to **7.8μV** upon addition of saline, which indicates suitability for electrophysiology due to a **<10μV** average **[9]**.

EIS was additionally utilized to assess the performance of the temperature-sensing IDE (**Figure 3 C&D**). After calibration through IR imaging confirmation (data not shown), temperature variations were assessed utilizing the attached microheater to vary DPBS temperatures. For the characterization of the thermal IDE sensor, previous impedance studies indicated that the solution resistances (R_s) and charge transfer resistances (R_{ct}) are more prevalent at higher frequencies, along with some impact at the at lower frequencies **[9,10]**. Lower frequencies however are often impacted by environmental noises, leading to necessarily complex post-processing to interpret data. Thus, higher frequencies would produce reliable physiologically relevant temperature change metrics across the room temperature to physiological range (22°C-42°C) tested. Decreases in impedance were expected due to increased ionic species motility in the saline solution when subject to higher temperatures. This would also be expected in salt-containing cell culture-media. If temperatures of interest were much higher, then an rapid increase in impedance would be expected due to increased concentrations of ionic species, resulting from evaporative effects. Performing ΔR/R analysis of the high frequency

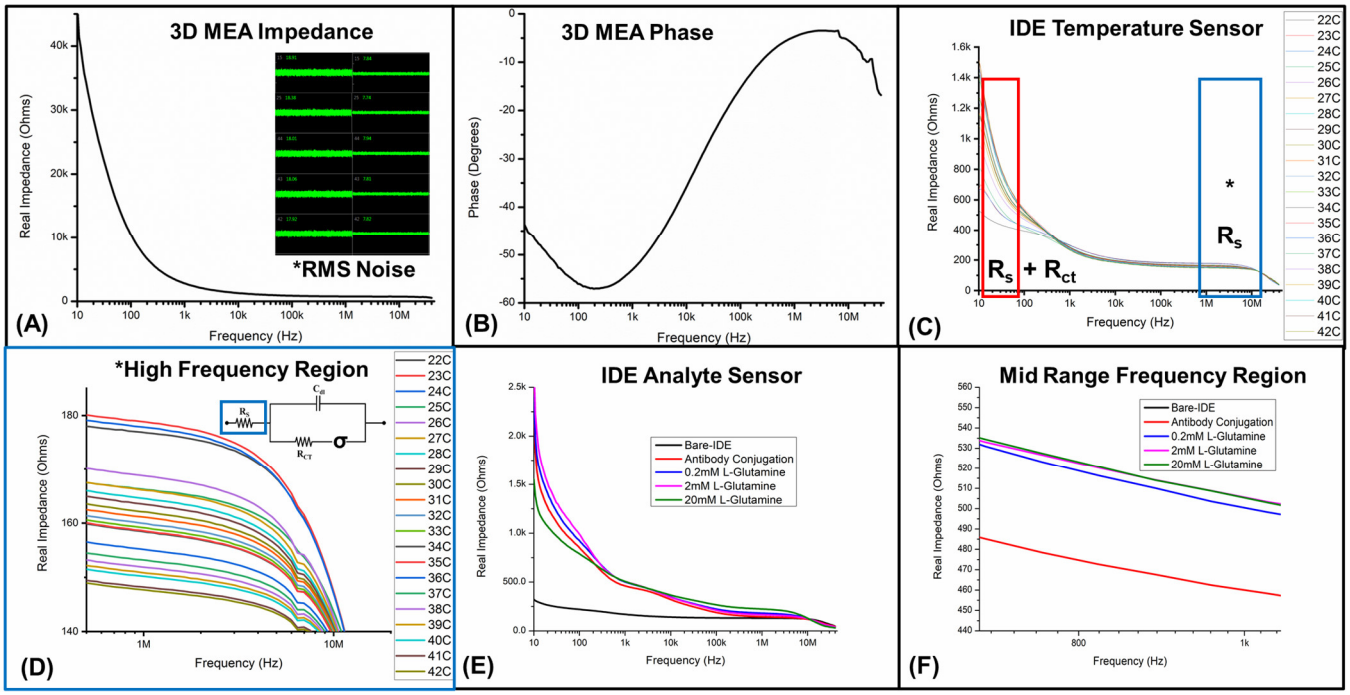

Figure 3: *Electrical impedance-based characterization of the 3D MEA, temperature, and analyte IDE sensors. (A&B) Full spectrum impedance and phase measurements of the 3D MEA structures. The 1kHz impedance of* ***2.76 kΩ****, and a phase signature of* ***-55°*** *are well within literature defined values* ***[9,10]****. (C&D) Impedance-based characterization of the temperature sensing IDE, utilizing the attached microheater to vary DPBS temperatures. (E&F) Impedance-based characterization of the analyte-sensing IDE. 1kHz impedance readings illustrate an increase as expected due to the added components atop the IDE.*

regions allowed for a better examination of impedance trends, to address if this hypothesis would hold true. A reliable trend was observed from the regression value of R^2***=0.975*** across all temperatures and illustrated a linear decrease of these impedance values at higher frequencies (1-10MHz) **[9,10]** across the physiologically relevant (**22°C-42°C**) temperatures. ΔR/R analysis for the aforementioned low frequency region were also assessed in a similar manner, however, the observed regression value (R^2***=0.660***) confirmed the unsuitability of the lower frequencies (10Hz-500Hz) for temperature sensing. These results serve to validate the utilization of the IDE sensor at higher frequencies, as a method for temperature sensing in the penta-modal 3D MEA platform. The relative success of the sensors performance for temperature applications near room temperature, it should be noted, did deviate slightly from expected results. Contextually however, the irregular temperature readings did occur near "room temperature" (22°C-25°C), which are less relevant for maintaining cellular homeostasis, and may be addressed through adjustments to sensitivity in future iterations. Additionally, creation of a calibration curve for this sensor would enable for software corrections in practical applications, as a strictly impedimetric reading serves as proof of its utility for potential signal differentiation.

Similarly, for analyte-sensing IDEs, impedance spectroscopy could be utilized to detect differential readings as the conjugation state of the sensor was adjusted (**Figure 3 E&F**). For sensing biologically relevant analytes, we determined that mid-range frequencies (600Hz-1.1kHz) exhibited the potential for reliable recordings. While the frequency of interest may vary in analyte detection **[11]**, our impedance readings around the 1kHz frequency for the chosen application, exhibited an increase in impedance. This was expected due to biological conjugation atop the IDE, which led to a modified capacitance value **[12]**. The double layer capacitance (C_{DL}) of the electrode system is expected to heavily impact the overall impedance values expressed around 1kHz **[9]**, and this should in fact be mirrored by a decrease in the phase values. Both of these trends were observed. Regression values from the ΔR/R plot, and the calculated R^2***=0.822*** provides an affirmative indication of its effectiveness. Of note, the 2mM and 20mM L-Glutamine concentrations appeared to potentially have reached the saturation point of this sensor ability to detect the antibody assay, which could be improved through conjugation chemistries, and/or adjustments in antibody solution concentration.

Figure 4 contains the SEM, AFM imaging of the IDE conjugation state and cells imaged on the Penta-Modal MEA. SEM image of the Ti/Au IDE along with a 3D microelectrode of the assembled device from **Figure 1J,** can be observed in **Figure 4A**. The enhanced SEM image in **Figure 4B** details the presence of conjugated antibodies on the Au IDE surface. **Figure 4C** is an AFM image of the unconjugated surface, which has a minimal surface roughness (**<12nm**) due to solely the evaporated metal. This is contrasted with **Figure 4D** which contains the conjugated antibodies. Larger roughness (**<66nm**) can be observed in this image, illustrating the functionalization of the IDE surface. However, this image additionally shows how a simple plasma treatment regimen can be used to avoid complex conjugation chemistries. **Figure 4 E-G** contains the optical and fluorescent imaging of C2C12 myocyte cells on the device at 5 days *in vitro* (DIV), demonstrating the optical clarity of the device. Calcein AM, and Propidium Iodide were utilized for live/dead cell viability, and to validate the transparency of the device for fluorescent imaging.

CONCLUSIONS

In this work, we demonstrated a combinatorial approach to the realization of a penta-modal biosensor for the investigation of electrogenic cells. We incorporated the capabilities for electrophysiology (through 3D MEA integration), optical

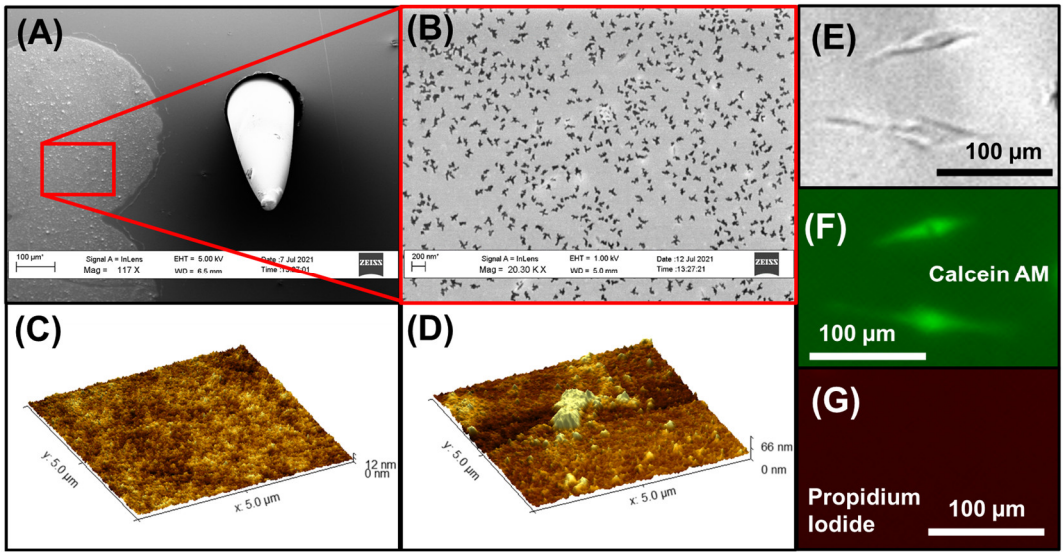

Figure 4: *Atomic Force Microscopy (AFM), Scanning Electron Microscopy (SEM), and fluorescent imaging of various parts of the device and cell assay. (A) SEM image of the Ti/Au IDE along with a 3D microelectrode of the assembled device from Figure 1J. (B) Enhanced SEM image of the conjugated antibodies on the Au IDE surface. (C&D) AFM images of the IDE showing the unconjugated surface of the IDE (C), which has a minimal surface roughness (**<12nm**) due to the evaporated metal. This is contrasted with (D) which contains the conjugated antibodies. Larger roughness (**<66nm**) can be observed in this image, illustrating the functionalization of the IDE surface. (E-G) Optical and fluorescent imaging of C2C12 myocyte cells on the device at 5 DIV, demonstrating the optical clarity of the device. (E) Optical imaging of the cells. (F) Calcein AM, live staining of the cells. (G) Propidium Iodide stain, for live/dead cell confirmation.*

interrogation (transparency), and microfluidic perfusion as established previously, and additionally enabled temperature and analyte sensing capabilities through impedimetric analysis of integrated IDEs on chip. Here, the 3D MEAs demonstrated comparable 1kHz performance and RMS noise to other devices reported in literature, and an alternate fabrication scheme to integrate microfluidic ports into the device were shown. The temperature sensor IDE successfully demonstrated the ability to sense different temperatures across the 22°C-42°C range, by utilizing higher frequency impedimetric analysis. An analyte sensing IDE was additionally demonstrated by utilizing a simple plasma-enhanced antibody conjugation protocol. Different concentrations of L-Glutamine were then sensed using the mid-frequency range from an impedance sweep. Finally, C2C12 myocytes were grown and imaged through the device, utilizing both optical and fluorescent means.

ACKNOWLEDGEMENTS

The authors would like to acknowledge funding provided through NIH UG3TR003150 grant, NSF EEC 2050266 (NSF REU O. S. Cepeda-Torres) and UCF ORC Doctoral Fellowship (C. M. Didier).

REFERENCES

[1] W. Anderson et al., *"Advances in 3D neuronal microphysiological systems: towards a functional nervous system on a chip,"* In Vitro Cellular & Developmental Biology-Animal, 2021.

[2] Q. Wu, et al. *"Organ-on-a-chip: Recent breakthroughs and future prospects,"* Biomedical engineering online, 2020.

[3] J. Freitas Orrico, et al. *"Fabrication and Characterization of 3D Microelectrode Arrays (3D MEAS) with Tri-Modal (Electrical, Optical, and Microfluidic) Interrogation of Electrogenic Cell Constructs,"* 21st International Conference on Solid-State Sensors, Actuators and Microsystems (Transducers), 2021.

[4] C. Didier, et al. *"Development of in vitro 2D and 3D microelectrode arrays and their role in advancing biomedical research,"* Journal of Micromechanics and Microengineering, 2020.

[5] D. Nieto, et al. *"Laser microfabrication of a microheater chip for cell culture outside a cell incubator,"* Colloids and Surfaces B: Biointerfaces, 2017.

[6] M. Kondzior, et al. *"Antibody-electroactive probe conjugates based electrochemical immunosensors,"* Sensors, 2014.

[7] N. Rusli, et al. *"Miniaturized Electrochemical Device for In-Situ Monitoring of Glucose, Lactate, Dissolved Oxygen, PH, and Temperature in Yeast Culture,"* 21st International Conference on Solid-State Sensors, Actuators and Microsystems (Transducers). IEEE, 2021.

[8] A. Baldwin, et al. *"An electrochemical impedance-based thermal flow sensor for physiological fluids,"* Journal of Microelectromechanical Systems, 2016.

[9] D. Borkholder. *"Cell-based biosensors using microelectrodes,"* Stanford University Thesis, 1999.

[10] S. Rajaraman. *"Micromachined three-dimensional electrode arrays for in-vitro and in-vivo electrogenic cellular networks,"* Georgia Institute of Technology Thesis, 2009.

[11] M. Strong, et al. *"Faradaic electrochemical impedance spectroscopy for enhanced analyte detection in diagnostics,"* Biosensors and Bioelectronics, 2021.

[12] S. MacKay, et al. *"Using impedance measurements to characterize surface modified with gold nanoparticles,"* Sensors, 2017.

CONTACT

*Swaminathan Rajaraman, tel: +1-407-823-4339; Swaminathan.Rajaraman@ucf.edu